Article ID: 1000-324X(2022)06-0683-08 **DOI:** 10.15541/jim20210652

Microstructure and Mechanical Properties of SiC Joint Brazed by Al-Ti Alloys as Filler Metal

XU Puhao, ZHANG Xiangzhao, LIU Guiwu, ZHANG Mingfen, GUI Xinyi, QIAO Guanjun

(School of Materials Science and Engineering, Jiangsu University, Zhenjiang 212013, China)

Abstract: SiC ceramic has excellent overall properties, and joining it to other materials with high joint strength is an important issue in the actual applications. Brazing of SiC ceramic to itself was performed using the as-fabricated Al-(10, 20, 30, 40)Ti alloys with nominal Ti concentrations of 10%, 20%, 30%, and 40% at 1550 ℃ × 30 min. The average joint shear strength fluctuates in the range of ~100–260 MPa with the interlayer thickness of ~50 μm. Moreover, the average strength SiC/Al-20Ti/SiC joint is increased markedly with the interlayer thickness decreasing from ~100 to 25 μm, reaching the maximum of ~315 MPa. Meanwhile, the (Al) phase in the interlayers is reduced gradually till disappear with the thinnest brazing interlayer, leaving the Al_4C_3, TiC and $(Al,Si)_3Ti$ phases in the interlayer. The joint fractures of SiC/Al-20Ti/SiC joint mainly occur in the SiC ceramic substrate near the interlayer/ceramic interface.

Key words: SiC; brazing; interfaces; microstructures; mechanical property

SiC ceramics are widely applied in many fields including aerospace, electronics, machinery, chemical and metallurgy industries due to the excellent overall properties, such as high strength, high hardness, high melting point, high thermal conductivity, low thermal expansion, as well as good oxidation, corrosion and thermal-shock resistances[1-2]. Indeed, joining of SiC ceramics to other materials is an important issue in these applications due to the inherent difficulties derived from the high degree of covalent bonding in SiC and the low self-diffusivity[3-4]. Presently, joining techniques of SiC ceramics are mainly involved in brazing, diffusion bonding, transient liquid phase bonding and reaction forming/bonding, *etc*[1]. Among them, the brazing, as the most convenient and highly efficient joining technique, can be divided into active metal brazing[5-7], low activation brazing[8-9] and air reactive brazing[10], *etc*.

Pure metals can react with SiC to form silicide+graphite, Si+carbide, silicide+carbide, and even ternary compounds[11]. Some pure metals (such as Ti, Cr, and Zr) that can produce silicide and carbide simultaneously or ternary compound by reaction with SiC, are commonly deemed as active metals for joining of SiC ceramics. These active metals were added in pure metals or alloys to form the brazing fill metals, involving binary[5,9,12-15], ternary[6,16-20], quaternary[21-24] and other multi-elemental alloys[7,25]. Valenza, *et al.*[5] performed the pressureless joining of sintered SiC to itself using Al-25Ti alloy as filler metal by capillary infiltration and using the Al_3Ti paste/Ti foil/Al_3Ti paste as interlayer at 1500 ℃ for 10 min, and obtained average joint shear strength of 296 and 89 MPa for single lap offset and torsion tests, respectively. Moreover, the additions of these active metals were mainly performed by means of film and coating besides alloying, such as Ti film[26-27] and Cr coating[20]. In addition, in order to reduce the residual thermal stress in joint, some inorganic particulates or nanoplatelets (involving B_4C, SiC, Cr_3C_2, *etc*.) with low coefficient of thermal expansion were introduced into Ag-Cu-Ti or Si-Ti alloys to form composite fillers for brazing of SiC ceramics[28-32]. Recently, the Ti_3SiC_2 MAX phase was also developed as the filler material for joining SiC[33-34] due to the high strength and thermal stability[35].

As mentioned above, several brazing methods and many brazing filler metals were explored for brazing of SiC ceramics, and some high-strength SiC/SiC joints were obtained too. However, it is quite difficult to optimize the joint strength and high-temperature resistance

Received date: 2021-10-22; **Revised date:** 2022-01-19; **Published online:** 2022-01-24
Foundation item: National Natural Science Foundation of China (52002153, 51572112); Natural Science Foundation of the Jiangsu Higher Education Institutions of China (20KJB430004); Key R&D Plan of Jiangsu Province (BE2019094)
Biography: XU Puhao (1993–), male, PhD candidate. E-mail: 13667004282@163.com
徐谱昊(1993–), 男, 博士研究生. E-mail: 13667004282@163.com
Corresponding author: LIU Guiwu, professor. E-mail: gwliu76@ujs.edu.cn; QIAO Guanjun, professor. E-mail: gjqiao@ujs.edu.cn
刘桂武, 教授. E-mail: gwliu76@ujs.edu.cn; 乔冠军, 教授. E-mail: gjqiao@ujs.edu.cn.

simultaneously, which lies on the brazing filler or interlayer composition and brazing process to a great extent. For example, Liu, *et al.*[6] investigated the active metal brazing of sintered SiC using Ag-35.25Cu-1.75Ti as the brazing filler material at 860–940 ℃ for 10–60 min, and obtained the optimal average joint strength of over 340 MPa at room temperature, but these joints can only endure temperature lower than 550 ℃. For this purpose, we fabricated four Al-Ti alloys with nominal Ti concentrations of 10%–40%(atom percent) and optimized the alloy composition and thickness based on the variation of room temperature shear strength of SiC/SiC brazed joint, and especially investigated the microstructure and phase evolution of joint interlayers for establishing the relationship between joint microstructure and performance. Actually, the four Al-Ti/SiC systems present excellent wettability with contact angle less than 15°, as reported in our previous work[15].

1 Experimental

The commercial solid-phase sintered SiC ceramics with a purity of 98% and dimensions of ϕ20 mm×5 mm or ~3 mm×4 mm×17 mm (Henan Aryan New Materials Co., Ltd.) were used as substrate for brazing experiments. The pure Al (≥99.999%) and Ti particles (≥99.995%) were used as raw materials for preparation of Al-Ti alloys. In order to remove the oxygen in the cavity of the melting equipment (DHL-300, Shenyang Scientific Instrument Co., LTD., Chinese Academy of Sciences), pure Ti particles of 30 g were placed in one of crucibles during the first refining, and four kinds of Al-Ti alloys with nominal Ti concentrations of 10%, 20%, 30% and 40% (atom percent) (Al-(10, 20, 30, 40)Ti) were fabricated by vacuum arc refining for 5 times, respectively. The resulting bulk Al-Ti alloys were processed by wire-electrode cutting and/or grinding into foils with different thicknesses, and then tailored into circular foils of ϕ20 mm. The microstructures and phase compositions of four Al-Ti alloys were characterized and analyzed by scanning electron microscope (SEM) coupled with energy dispersive spectroscope (EDS) and X-ray diffraction (XRD).

Before brazing, the brazing surfaces of SiC ceramics and the alloy foils were ground, polished and then ultrasonically cleaned in alcohol. Two SiC pieces or bars and one alloy foil were assembled together in a graphite mold and then vacuum brazed in a sintering furnace (High-multi 5000, Japan) at ~7 mPa. The pressure ~20 kPa was applied to the top of the SiC/Al-Ti/SiC couples. For the brazing cycle, the furnace was firstly heated from room temperature to 1200 ℃ at 20 ℃/min. Subsequently, the temperature of furnace was further raised to 1500 ℃ at 10 ℃/min and then raised to 1550 ℃ at 5 ℃/min and held for 30 min. Then, the joint sample was cooled down to 300 ℃ at rate of ~3 ℃/min and finally furnace- cooled to room temperature. To evaluate the shear strength of brazed joints, these SiC/SiC joints were cut into specimens of ~10 mm×10 mm×5 mm, and then the resulting joints were cross-sectioned, polished and observed to investigate the microstructure and phase evolution of joint cross-sections by SEM coupled with EDS. In particular, a thin Al-20Ti/SiC interface sample was cut from a cross-sectioned SiC/Al-20Ti/SiC joint by using focus ion beam (FIB) and observed by transmission electron microscope (TEM). The joint shear strength was evaluated by a shear test method using a DDL100 electronic universal testing machine at the loading speed of 0.5 mm/min with clamp and assemble chart shown in Fig. S1. Furthermore, the three-point bending specimens with span of 26 mm were used to characterize the high-temperature resistance of the typical SiC/Al-20Ti/SiC brazed joint on an AG-X plus mechanical testing system under Ar atmosphere. The joined specimens were firstly heated to the testing temperature (800 ℃) at a rate of ~33.3 ℃/min and held for ~7 min, and then the three-point bending test was carried out. The mean value of joint shear strength was obtained from the arithmetical average of 4 samples. The microstructures and phase compositions of joint fracture surfaces were examined and analyzed by SEM coupled with EDS and XRD. The manufacturing, testing and characterization methods of joint shear samples were similarly described in our precious reports[36].

2 Results and discussion

2.1 Brazing alloys

Fig. 1 shows the BSE images of the nominal Al-(10, 20, 30, 40)Ti alloys, and Fig. 2 shows their XRD patterns. The elemental distributions were also determined by the EDS mapping of the four alloys (Fig. S2). The actual Ti concentrations of the four nominal Al-(10, 20, 30, 40)Ti alloys, determined by EDS, are 12.62%, 20.45%, 28.61% and 38.26% (atom percent), respectively. By combining the XRD patterns, EDS mapping and Al-Ti binary phase diagram[5], the bright and dark phases are Al_3Ti and Al for Al-(10, 20)Ti alloys (Fig. 1(a, b), and Fig. S2), while the bright and gray phases are Al_2Ti and Al_3Ti for the Al-30Ti alloy (Fig. 1(c), Fig. 2 and Fig. S2). Moreover, the Al-40Ti alloy is composed of AlTi (bright phases) and Al (gray intergranular phases, determined by the EDS in Fig. S3) although the Al phase is not detected in

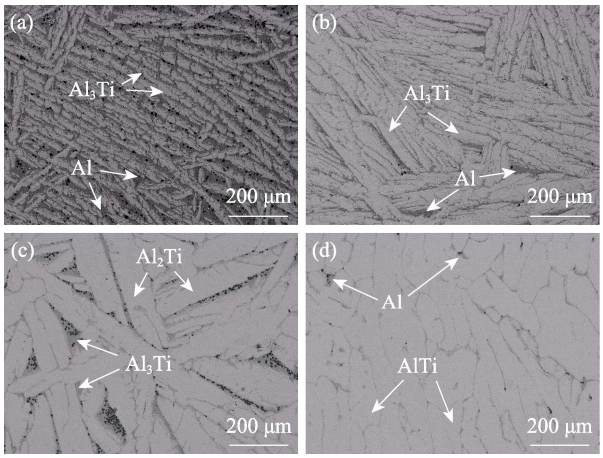

Fig. 1　BSE images of four nominal Al-Ti alloys
(a) Al-10Ti; (b) Al-20Ti; (c) Al-30Ti; (d) Al-40Ti. The black dots are the diamond particles introduced during the polishing

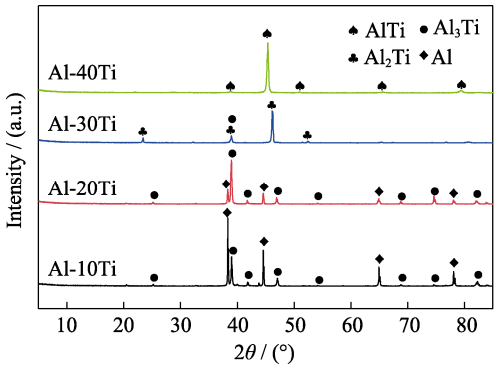

Fig. 2　XRD patterns of Al-Ti alloys

the XRD pattens (Fig. 2) due to amount in Al-40Ti alloy. The main phase composition of Al-Ti alloys gradually transforms from Al, Al_3Ti, Al_2Ti to AlTi with the Ti concentration increasing from 10% to 40%.

2.2　Joint microstructure evolution

Fig. 3 shows the cross-sectional BSE images of SiC/SiC joints brazed using four nominal Al-(10, 20, 30, 40)Ti alloys with interlayer thickness of ~50 μm and the EDS elemental mapping of SiC/Al-20Ti/SiC joint cross-section, and Table 1 lists the EDS results of main phases on the joint cross-sections. As shown in Fig. 3(a, b), the interlayer of SiC/Al-10Ti/SiC joint is composed of (Al), TiC and $(Al,Si)_3Ti$ phases, and the TiC and (Al) phases are mainly distributed at the Al-10Ti/SiC interfaces and in the middle of interlayer, respectively, while the scattered $(Al,Si)_3Ti$ grains is embedded in the (Al). However, the three phases, (Al), TiC and $(Al,Si)_3Ti$, are evenly distributed in the interlayer when Al-20Ti alloy is used as brazing filler metal (Fig. 3(c, d)), which contribute to the improvement of joint strength.

The residual (Al) phase in two interlayers of SiC/Al-10Ti/SiC and SiC/Al-20Ti/SiC joints is mainly attributed to the high concentration of Al in Al-10Ti and Al-20Ti alloys. Compared with Al-10Ti, the (Al) phase in original Al-20Ti is sharply decreased, leaving discrete (Al) in the interlayer after the serious interfacial

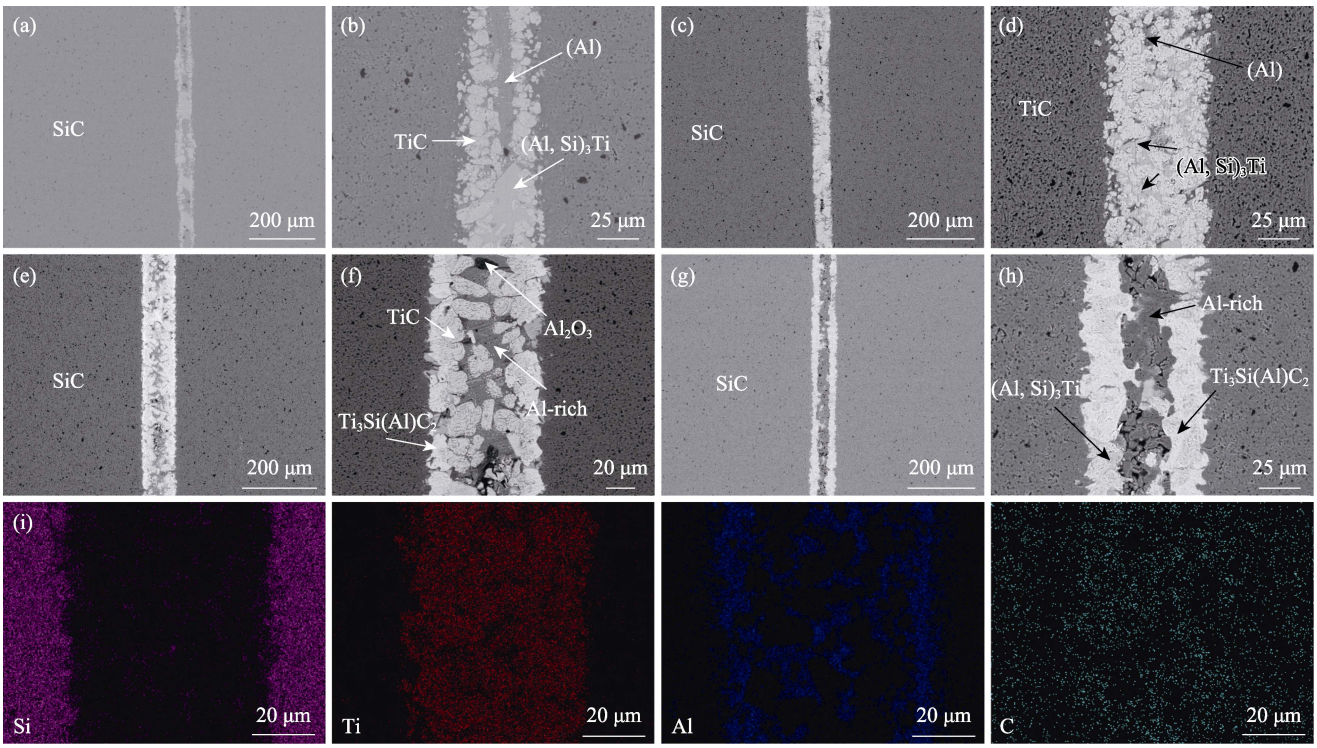

Fig. 3　Cross-sectional BSE images of SiC/SiC joints brazed using the four nominal Al-Ti alloys (a–h) and corresponding EDS elemental mapping (i)
(a, b) Al-10Ti; (c, d) Al-20Ti; (e, f) Al-30Ti; (g, h) Al-40Ti

Table 1 EDS results of partial phases in joint interlayers (atom percent)

Data from	Elemental composition /%				Possible phases
	Ti	Al	C	Si	
Fig. 3(b)	0.87	98.04	–	1.09	(Al)
	55.33	–	45.67	–	TiC
	25.85	62.83	–	11.32	$(Al,Si)_3Ti$
Fig. 3(d)	–	98.91	–	1.09	(Al)
	53.98	0.06	45.11	0.84	TiC
	26.27	59.23	2.47	12.03	$(Al,Si)_3Ti$
Fig. 3(f)	48.61	1.85	31.39	18.15	$Ti_3Si(Al)C_2$
Fig. 3(h)	50.29	1.26	30.42	18.03	$Ti_3Si(Al)C_2$

interactions (Fig. 3(d)). EDS elemental mapping images further demonstrate the relatively uniform elemental distributions and elemental compositions of main phases in the joint cross-sections (Fig. 3(i)). Surprisely, a dark Al-rich layer involving (Al) solid solution and Al_2O_3 phases is located in the middle of interlayers while employing the other two Al-Ti alloys with higher Ti concentrations (Fig. 3(e–h)), which is obviously different from the cross-sectional microstructures in previous report [5]. The formation of Al-rich layer can be derived from the formation of a large amount of Ti_3SiC_2 MAX phase, which consumes a lot of Ti, Si and TiC [37]. The elemental and phase distributions were further demonstrated by the typical EDS mapping of SiC/Al-30Ti/SiC joint (Fig. S4). As a result, the TiC content increases gradually and then decreases with the Ti concentration increasing from 10% to 40%.

Fig. 4 shows the cross-sectional BSE images of SiC/SiC joints brazed using the nominal Al-20Ti alloys with interlayer thicknesses of 25–100 μm. As shown in Fig. 4, no Al-rich layer nor $Ti_3Si(Al)C_2$ phase can form on the cross-sections of joints, and the (Al) phase decreases gradually till disappear with the interlayer thickness decreasing from ~100 μm to 25 μm. Undoubtedly, the absence of low melting point of (Al) phase can contribute to the high-temperature resistance of SiC/SiC brazed joints. Moreover, some cracks are produced in the ceramic substrate near the interface (Fig. 4(d)), which can bring a negative effect on the joint strength. To clarify the interfacial microstructure and phase composition of the SiC/Al-20Ti/SiC joint sample with the thinnest interlayer, a HRTEM analysis was performed on the Al-20Ti/SiC interface sample prepared by means of FIB. As shown in Fig. 5 and Fig. S5, some bright and dark phases can co-exist at the interlayer/SiC interfaces, which can be determined as TiC and Al_4C_3 with interplanar spacings of 0.2164 and 0.1787 nm according to HRTRM analyses and their SAED patterns, resulting in formation of TiC/SiC and Al_4C_3/TiC interfaces. Meanwhile, some $(Al,Si)_3Ti$ phases are formed near the TiC and Al_4C_3 phases according to the EDS elemental mapping (Fig. S5). A microcrack is also observed due to the difference of coefficient of thermal expansion (CTE) between the TiC and $(Al,Si)_3Ti$ phases, which can reduce the joint strength to a certain degree.

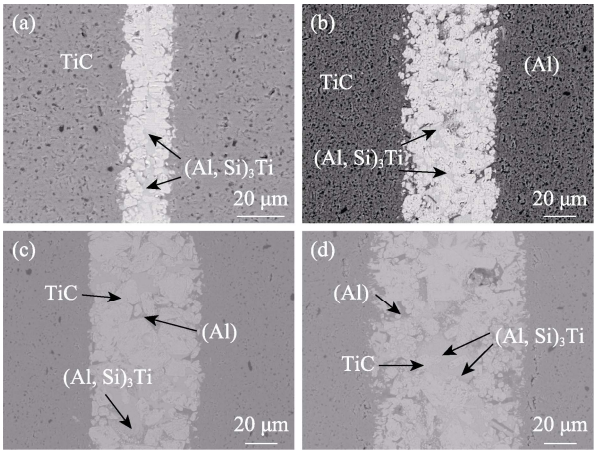

Fig. 4 Cross-sectional BSE images of SiC/Al-20Ti/SiC joints brazed with interlayers of different thickness
(a) ~25 μm; (b) 50 μm; (c) 70 μm; (d) 100 μm

2.3 Joint microstructure evolution

Fig. 6 shows the variations of joint shear strength with the Ti concentration of Al-Ti alloys and the interlayer thickness of Al-20Ti alloy. The average joint shear strength fluctuates in the range of ~100–260 MPa with the Ti concentration of Al-Ti alloys increasing from 10% to 40% (Fig. 6(a)). Considering the interlayer thickness of ~50 μm, the optimal SiC/SiC brazed joint with the maximum average joint strength of 266 MPa is obtained when using the Al-20Ti alloy as brazing filler metal, namely that the highest joint strength is mainly attributed to the lowest thermal stress generated from the uniform phase distribution (Fig. 3(d, i)). Furthermore, the average joint strength is increased markedly with the interlayer thickness decreasing from ~100 μm to 25 μm, arriving at the maximum of ~315 MPa, which is comparable to that of the SiC joint brazed using Al-25Ti alloy as filler material [5]. Similarly, this variation of joint strength with interlayer thickness is related to the interlayer microstructure and phase composition. The absence of (Al) phase in the interlayer is contribute to the improvement of joint strength based on the formation of residual thermal stress due to the difference of CTE between the SiC substrate and interlayer composition materials, where the CTEs of SiC, Al_3Ti, TiC, Ti_3SiC_2 and Al are 4.70×10^{-6}/℃, $(3.9–4.2)\times10^{-6}$/℃, 7.40×10^{-6}/℃, 8.87×10^{-6}/℃ and 23.21×10^{-6}/℃, respectively [5,37]. On the other hand, the possibility of emerging cracks during the shear test is reduced sharply with the interlayer thickness decreasing,

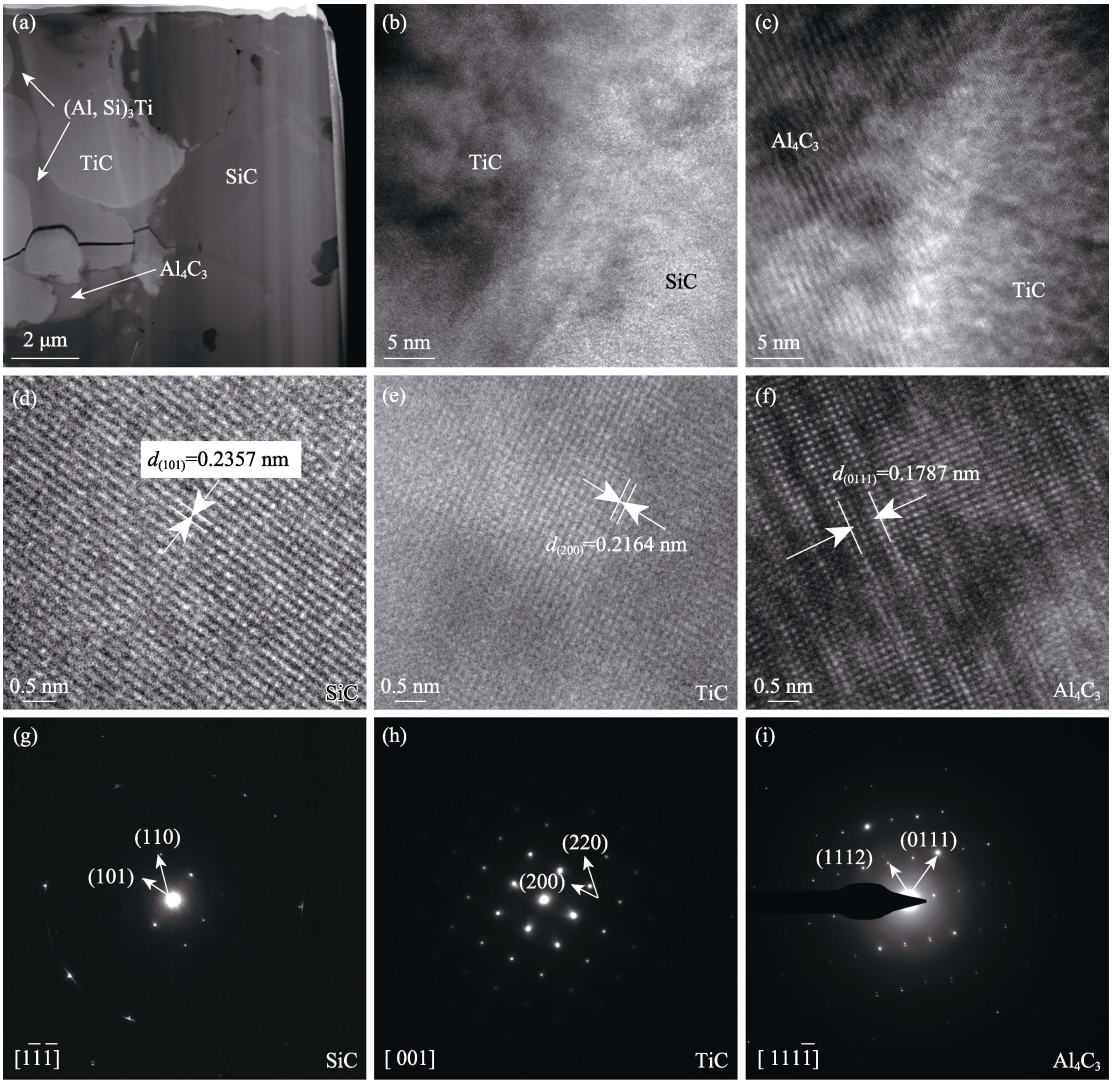

Fig. 5　Interfacial (a) TEM and (b–f) HRTEM images of SiC/Al-20Ti/SiC joint sample with interlayer thickness of ~25 μm and the corresponding (g–i) SAED patterns

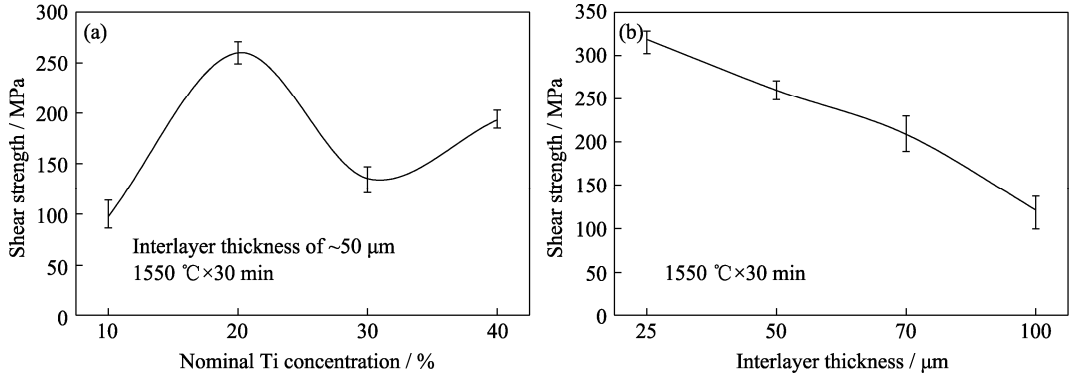

Fig. 6　Variations of joint shear strength with (a) Ti concentration of Al-Ti alloys and (b) interlayer thickness of Al-20Ti alloy

and thus the joint strength trends to increase. Actually, the joint 3-point bending strength of SiC/Al-20Ti/SiC brazed joint can reach ~53 MPa at 800 ℃, indicating that the brazed joint presents a good high-temperature resistance.

Fig. 7 and Fig. 8 show the typical fracture surface morphologies of SiC/SiC joints brazed using four nominal Al-Ti alloys and the corresponding XRD patterns of fracture surfaces. It is found that the joint fractures mainly occur in the interlayer, in the SiC ceramic substrate and at the Al-Ti/SiC interface during the shear test. From Fig. 7(a, b), one of the SiC/Al- 10Ti/SiC joint fractures occurs in the SiC ceramic substrate, with the fracture path passing across the interlayer, leaving the

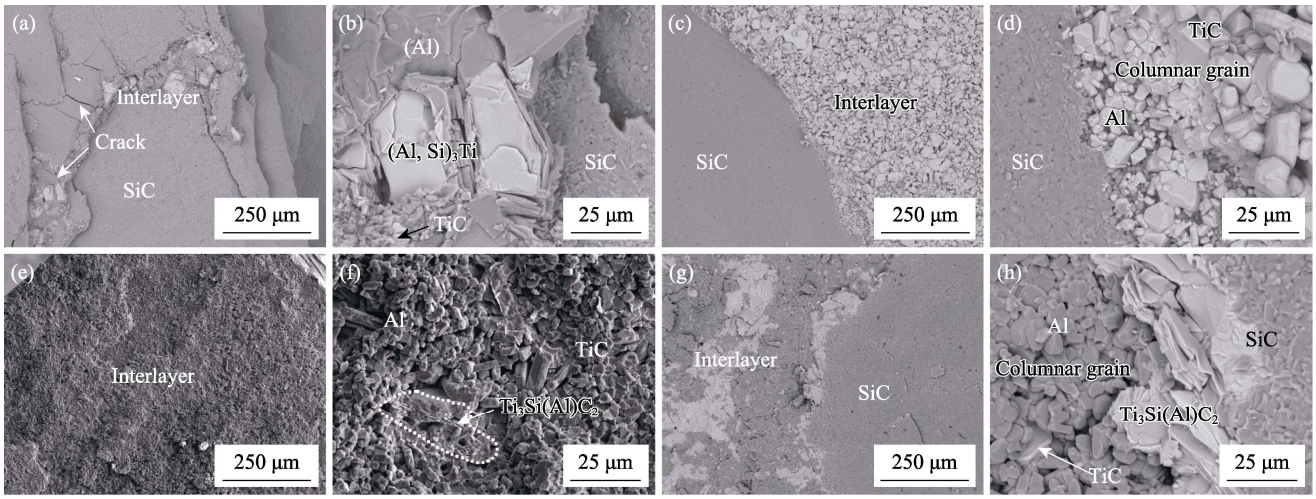

Fig. 7 Typical fracture surface morphologies of SiC/SiC joints brazed using different nominal Al-Ti alloys
(a, b) Al-10Ti; (c, d) Al-20Ti; (e, f) Al-30Ti ; (g, h) Al-40Ti

(Al), $(Al,Si)_3Ti$ and TiC on the fracture surface (Fig. 8). These cracks originated from the difference of CTE among the newly formed phases can reduce the joint strength. Most of the SiC/Al-20Ti/SiC joint fractures occur in the SiC ceramic substrate near the interlayer/ceramic interface, showing good interfacial bonding. However, only one SiC/Al-20Ti/SiC joint with interlayer thickness of ~50 μm breaks off at the interface, with the crack going along the interlayer partially (Fig. 7(c)), leaving only TiC on the fracture surface (Fig. 8). Moreover, all the SiC/Al-(30, 40)Ti/SiC joint fractures take place in the interlayer (Fig. 7(e)) or at the Al-Ti/SiC interface. Moreover, the cracks in the interlayer are reduced sharply with the Ti content increasing, thus showing an increasing trend of joint strength. For instance, one of the SiC/Al-40Ti/SiC joint fractures initiates in the interlayer and ends at the Al-Ti/SiC interface, exposing the laminated $Ti_3Si(Al)C_2$, columnar TiC and near-equiaxial Al grains (Fig. 7(g, h) and Fig. 8). The TiC and Al phases with special morphologies are mainly attributed to the crystal nucleation and growth during the whole brazing process and cooling, respectively.

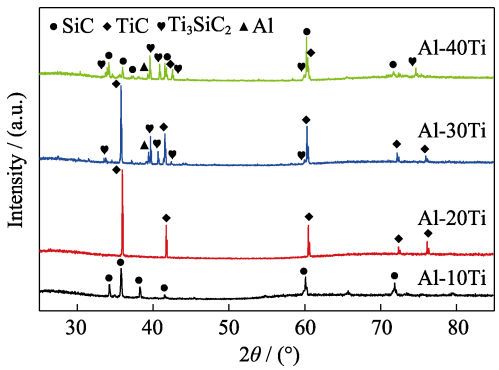

Fig. 8 XRD patterns of fracture surfaces of SiC/SiC joints brazed using various nominal Al-Ti alloys

3 Conclusions

Brazing of SiC ceramic to itself was performed using as-prepared Al-Ti alloys as filler metals and the microstructure, phase evolution and shear strength of the brazed joint were discussed. Considering the interlayer thickness of ~50 μm, the uniform phase distribution is only observed in the SiC/Al-20Ti/SiC joint, and the $Ti_3Si(Al)C_2$ MAX phase can form at the Al-(30, 40)Ti/SiC interfaces. The (Al) phase in the interlayer decreases gradually till disappear with the interlayer thickness decreasing from ~100 μm to 25 μm when the Al-20Ti alloys is used as filler metal. The average joint shear strength fluctuates in the range of 100–260 MPa with the interlayer of ~50 μm. The average strength SiC/Al-20Ti/SiC joint is increased markedly with the interlayer thickness decreasing from ~100 μm to 25 μm, reaching the maximum of ~315 MPa. Most of SiC/Al-20Ti/SiC joint fractures occur in the ceramic substrate near the interlayer/ceramic interface, while those of SiC/Al-(10, 30, 40)Ti/SiC joints appear in the interlayer, at the interface and in the SiC ceramic substrate with the crack crossing the interlayer.

Supporting Materials

Supporting materials related to this article can be found at https://doi.org/10.15541/jim20210652.

References:

[1] LIU G W, ZHANG X Z, YANG J, *et al*. Recent advances in joining of SiC-based materials (monolithic SiC and SiC_f/SiC composites): joining processes, joint strength, and interfacial behavior. *Journal of Advanced Ceramics*, 2019, **8(1):** 19–38.
[2] ZHAO S, YANG Z C, ZHOU X G. Fracture behavior of SiC/SiC

composites with different interfaces. *Journal of Inorganic Materials*, 2016, **31(1):** 58–62.

[3] FERNIE J, DREW R, KNOWLES K. Joining of engineering ceramics. *International Materials Reviews*, 2009, **54:** 283–331.

[4] YOON D H, REIMANIS I E. A review on the joining of SiC for high-temperature applications. *Journal of the Korean Ceramic Society*, 2020, **57(5):** 246–270.

[5] VALENZA F, GAMBARO S, MUOLO M L, *et al*. Wetting of SiC by Al-Ti alloys and joining by *in-situ* formation of interfacial $Ti_3Si(Al)C_2$. *Journal of the European Ceramic Society*, 2018, **38(11):** 3727–3734.

[6] LIU Y, HUANG Z R, LIU X J. Joining of sintered silicon carbide using ternary Ag-Cu-Ti active brazing alloy. *Ceramics International*, 2009, **35(8):** 3479–3484.

[7] XIONG H P, WEI M, XIE Y H, *et al*. Control of interfacial reactions and strength of the SiC/SiC joints brazed with newly-developed Co-based brazing alloy. *Journal of Materials Research*, 2007, **22(10):** 2727–2736.

[8] KOLTSOV A, HODAJ F, EUSTATHOPOULOS N. Brazing of AlN to SiC by Pr silicides: physicochemichal aspects. *Materials Science and Engineering: A*, 2008, **495(1/2):** 259–264.

[9] RICCARDI B, NANNETTI C A, WOLTERSDORF J, *et al*. Joining of SiC based ceramics and composites with Si-16Ti and Si-18Cr eutectic alloys. *International Journal of Materials & Product Technology*, 2004, **20(5):** 440–451.

[10] ZHAO S T, ZHAGN X Z, LIU G W, *et al*. Surface metallization of SiC ceramic by Mo-Ni-Si coatings for improving its wettability by molten Ag. *Rare Metal Materials and Engineering*, 2018, **47(3):** 759–765.

[11] LIU G W, MUOLO M L, VALENZA F, *et al*. Survey on wetting of SiC by molten metals. *Ceramics International*, 2010, **36(4):** 1177–1188.

[12] ZHAO H T, HUANG J H, ZHANG H, *et al*. Vacuum brazing of Si/SiC ceramic and low expansion titanium alloy by using Cu-Ti fillers. *Rare Metal Materials and Engineering*, 2007, **36(12):** 2184–2188.

[13] LI J K, LIU L, LIU X. Joining of SiC ceramic by 22Ti-78Si high-temperature rutectic brazing alloy. *Journal of Inorganic Materials*, 2011, **26(12):** 1314–1318.

[14] FU W, SONG X G, TIAN R C, *et al*. Wettability and joining of SiC by Sn-Ti: Microstructure and mechanical properties. *Journal of Materials Science and Technology*, 2020, **40:** 15–23.

[15] XU P H, GUI X Y, ZHANG X Z, *et al*. Wetting and interfacial behavior of Al-Ti/4H-SiC system: a combined study of experiment and DFT simulation. *Ceramics International*, 2021, **47:** 69–77.

[16] HAO Z T, WANG D P, YANG Z W, *et al*. Microstructural evolution and mechanical properties of $FeNi_{42}$ alloy and SiC ceramic joint vacuum brazed with Ag-based filler metals. *Ceramics International*, 2020, **46(8):** 12795–12805.

[17] PRAKASH P, MOHANDAS T, RAJU P D. Microstructural characterization of SiC ceramic and SiC-metal active metal brazed joints. *Scripta Materialia*, 2005, **52(11):** 1169–1173.

[18] TIAN W B, SUN Z M, ZHANG P, *et al*. Brazing of silicon carbide ceramics with Ni-Si-Ti powder mixtures. *Journal of the Australian Ceramic Society*, 2017, **53(2):** 511–516.

[19] SUDMEYER I, HETTESHEIMER T, ROHDE M. On the shear strength of laser brazed SiC-steel joints: effects of braze metal fillers and surface patterning. *Ceramics International*, 2010, **36(3):** 1083–1090.

[20] CHEN Z B, HU S P, SONG X G, *et al*. Brazing of SiC ceramics pretreated by chromium coating using inactive AgCu filler metal. *International Journal of Applied Ceramic Technology*, 2020, **17(6):** 2591–2597.

[21] LIU Y, ZHU Y Z, YANG Y, *et al*. Microstructure of reaction layer and its effect on the joining strength of SiC/SiC joints brazed using Ag-Cu-In-Ti alloy. *Journal of Advanced Ceramics*, 2014, **3(1):** 71–75.

[22] MOSZNER F, MATA-OSORO G, CHIODI M, *et al*. Mechanical behavior of SiC joints brazed using an active Ag-Cu-In-Ti braze at elevated temperatures. *International Journal of Applied Ceramic Technology*, 2017, **14(4):** 703–711.

[23] HE H M, LU C Y, HE H M, *et al*. Characterization of SiC ceramic joints brazed using Au-Ni-Pd-Ti high-temperature filler alloy. *Materials*, 2019, **12(6):** 931.

[24] QIN Q, ZHANG J, LU CJ, *et al*. Microstructure and mechanical properties of the SiC/Zr_4 joints brazed with TiZrNiCu filler for nuclear application. *Progress in Natural Science-Materials International*, 2018, **28(3):** 124–131.

[25] XIONG H P, WEI M, XIE Y H, *et al*. Brazing of SiC to a wrought nickel-based superalloy using CoFeNi(Si, B)CrTi filler metal. *Materials Letters*, 2007, **61(25):** 4662–4665.

[26] SONG X G, CHEN Z B, HU S P, *et al*. Wetting behavior and brazing of titanium-coated SiC ceramics using $Sn_{0.3}Ag_{0.7}Cu$ filler. *Journal of the American Ceramic Society*, 2019, **103(2):** 912–920.

[27] CHEN Z B, BIAN H, NIU C N, *et al*. Titanium-deposition assisted brazing of SiC ceramics using inactive AgCu filler. *Materials Characterization*, 2018, **142:** 219–222.

[28] DAI X Y, CAO J, CHEN Z, *et al*. Brazing SiC ceramic using novel B4C reinforced Ag-Cu-Ti composite filler. *Ceramics International*, 2016, **42(5):** 6319–6328.

[29] LIU Y, QI Q, ZHU Y, *et al*. Microstructure and joining strength evaluation of SiC/SiC joints brazed with SiC_p/Ag-Cu-Ti hybrid tapes. *Journal of Adhesion Science and Technology*, 2015, **29(15):** 1563–1571.

[30] LI Z, WEI R W, WEN Q, *et al*. Microstructure and mechanical properties of SiC ceramic joints vacuum brazed with *in-situ* formed SiC particulate reinforced Si-24Ti alloy. *Vacuum*, 2019, **173:** 109160.

[31] ZHONG Z H, HOU G X, ZHU Z X, *et al*. Microstructure and mechanical strength of SiC joints brazed with Cr_3C_2 particulate reinforced Ag-Cu-Ti brazing alloy. *Ceramics International*, 2018, **44(10):** 11862–11868.

[32] SONG Y Y, LIU D, HU S P, *et al*. Graphene nanoplatelets reinforced AgCuTi composite filler for brazing SiC ceramic. *Journal of the European Ceramic Society*, 2019, **39(4):** 696–704.

[33] ZHOU X B, LI Y B, LI Y F, *et al*. Residual thermal stress of SiC/Ti_3SiC_2/SiC joints calculation and relaxed by post-annealing. *International Journal of Applied Ceramic Technology*, 2018, **15:** 1157–1165.

[34] ZHOU X B, HAN Y H, SHEN X F, *et al*. Fast joining SiC ceramics with Ti_3SiC_2 tape film by electric field-assisted sintering technology. *Journal of Nuclear Materials*, 2015, **466:** 322–327.

[35] YANG D X, ZHOU Y, YAN X H, *et al*. Highly conductive wear resistant Cu/Ti_3SiC_2(TiC/SiC) co-continuous composites *via* vacuum infiltration process. *Journal of Advanced Ceramics*, 2020, **9(1):** 83–93.

[36] ZHANG X Z, LIU G W, TAO J N, *et al*. Brazing of WC-8Co cemented carbide to steel using Cu-Ni-Al alloys as filler metal: microstructures and joint mechanical behavior. *Journal of Materials Science and Technology*, 2018, **34(7):** 1180–1188.

[37] ZHOU X B, JING L, KWON Y D, *et al*. Fabrication of SiC_w/Ti_3SiC_2 composites with improved thermal conductivity and mechanical properties using spark plasma sintering. *Journal of Advanced Ceramics*, 2020, **9(4):** 462–470.

Al-Ti 合金钎焊 SiC 陶瓷接头界面微观结构与力学性能

徐谱昊, 张相召, 刘桂武, 张明芬, 桂新易, 乔冠军

(江苏大学 材料科学与工程学院, 镇江 212013)

摘 要: SiC陶瓷具有优异的综合性能, 通过钎焊获得高强度接头是其获得广泛应用的重要前提。研究采用Al-(10, 20, 30, 40)Ti(Ti 的名义原子含量 10%、20%、30%、40%)系列合金, 在 1550 ℃条件下, 对 SiC 陶瓷进行钎焊 30 min。当中间层厚度为~50 μm 时, SiC 钎焊接头的平均剪切强度处于 100~260 MPa 范围内。当采用 Al-20Ti 合金作为钎料时, 随着中间层厚度从~100 μm 减小至 25 μm, 钎焊接头的平均强度逐渐提高, 且最大强度~315 MPa。同时, 钎焊中间层中(Al)相逐渐减少直至消失, 只留下 Al_4C_3、TiC 和$(Al,Si)_3Ti$ 相。SiC/Al-20Ti/SiC 钎焊接头的断裂主要发生在靠近中间层/陶瓷界面位置的陶瓷基体内。

关 键 词: SiC; 钎焊; 界面; 微结构; 力学性能

中图分类号: TG456 **文献标志码**: A

Supporting materials:

Microstructure and Mechanical Properties of SiC Joint Brazed by Al-Ti Alloys as Filler Metal

XU Puhao, ZHANG Xiangzhao, LIU Guiwu, ZHANG Mingfen, GUI Xinyi, QIAO Guanjun

(School of Materials Science and Engineering, Jiangsu University, Zhenjiang 212013, China)

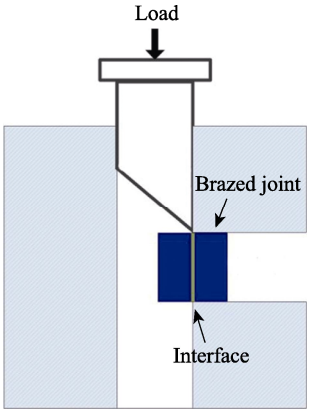

Fig. S1　Schematic of the shear test fixture

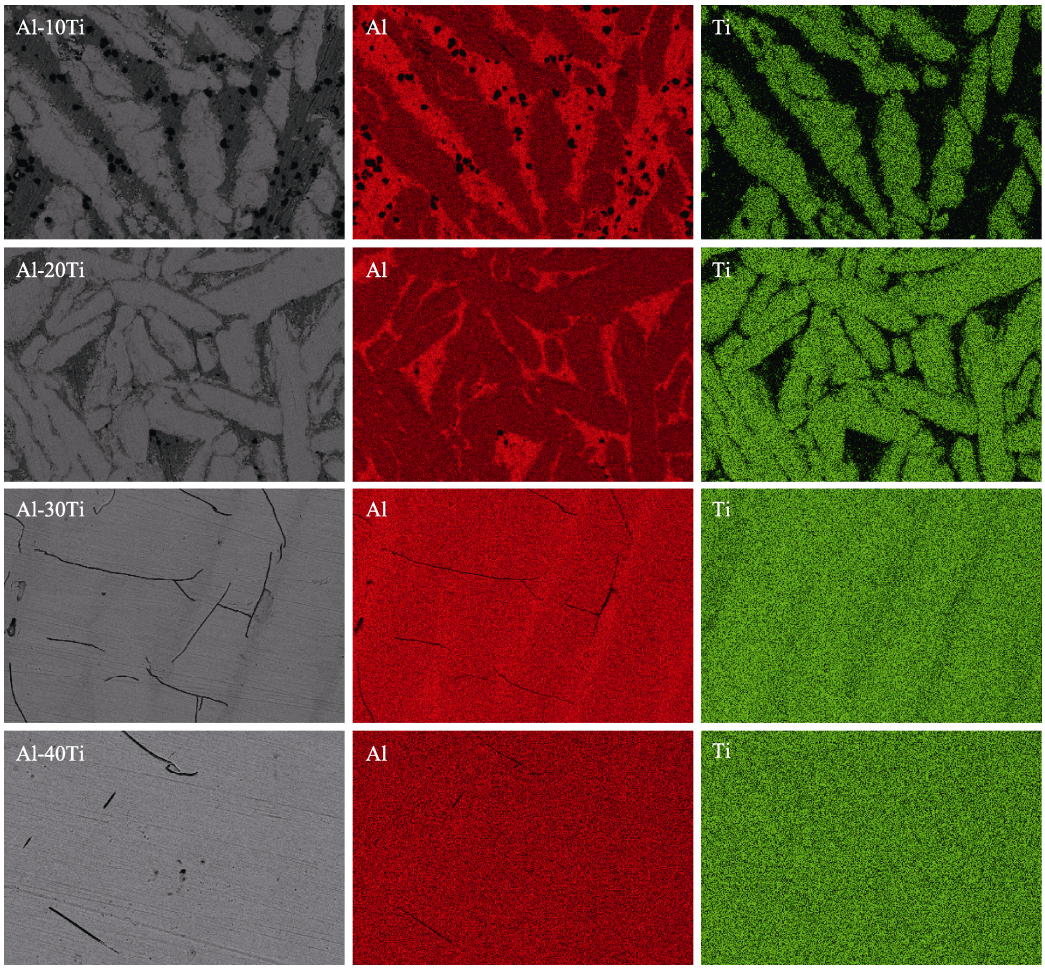

Fig. S2　Typical BSE images of Al-(10, 20, 30, 40)Ti alloys and the corresponding elemental mapping

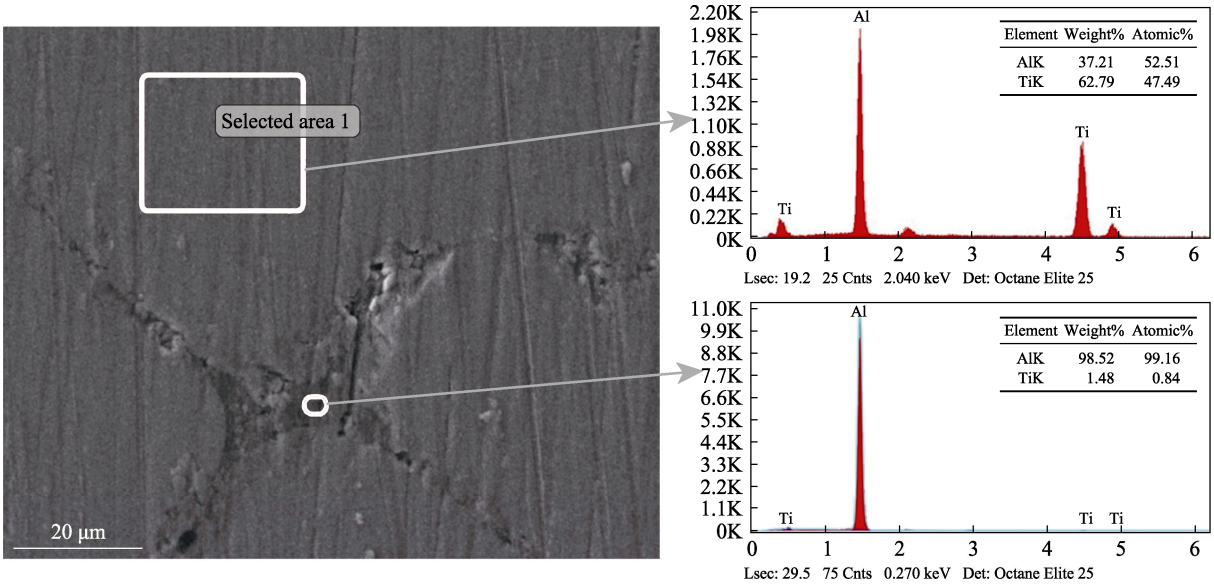

Fig. S3 Typical BSE image of Al-40Ti alloy and the corresponding elemental compositions of the selected area

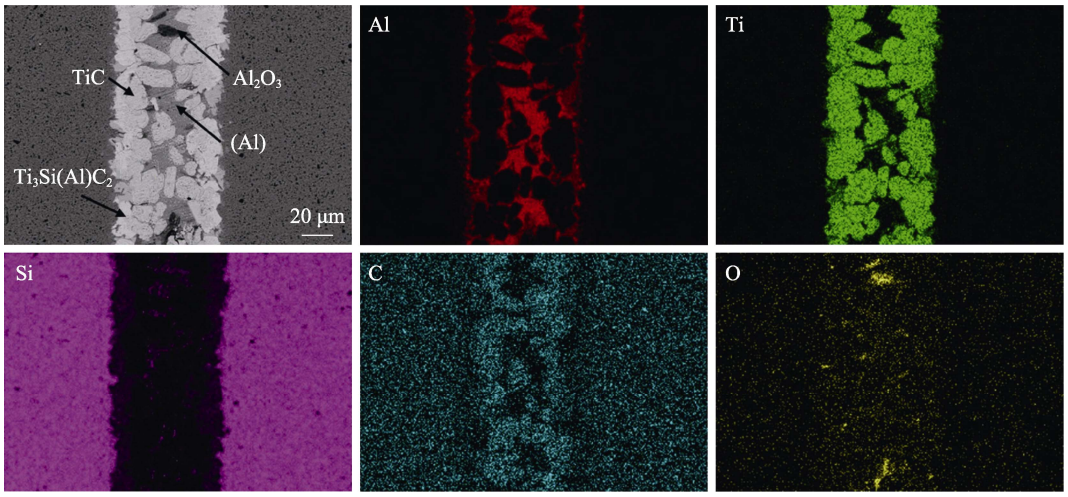

Fig. S4 Cross-sectional BSE image of the SiC/Al-30Ti/SiC joint brazed at 1550 ℃ × 30 min and the corresponding elemental mappings

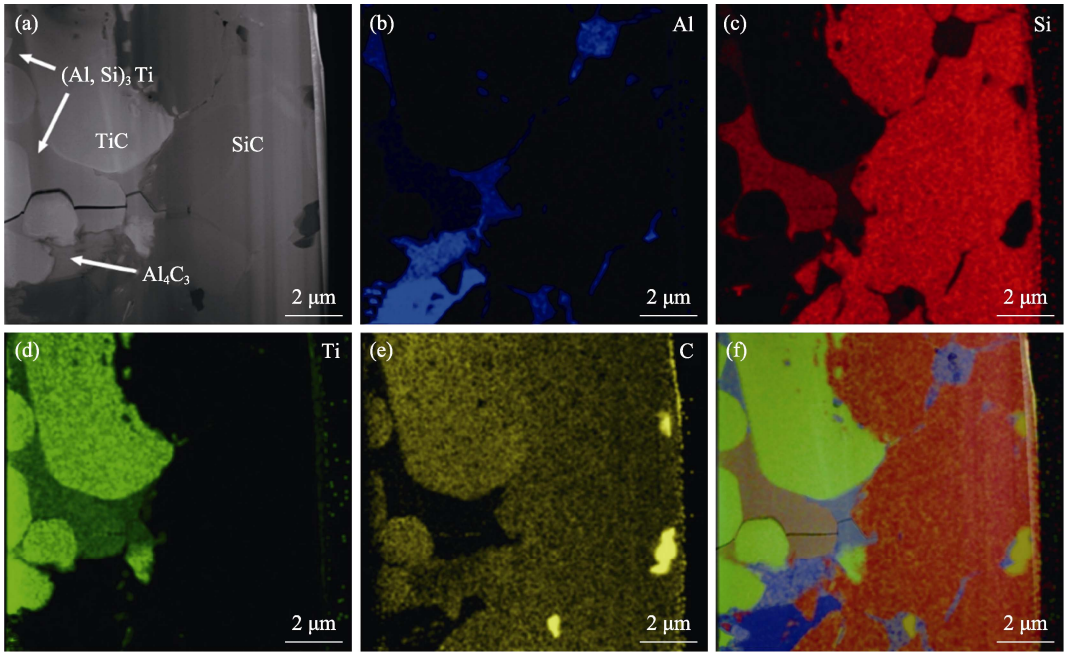

Fig. S5 Interfacial TEM image of SiC/Al-20Ti/SiC joint sample and the corresponding elemental mappings